Analysis of heat transfer in different CPC solar collectors: a CFD approach.

Abstract:

In this paper a methodology is proposed to estimate thermal heat losses inside compound parabolic collectors (CPC) to be used in designing and validating new collectors' concepts and materials. CFD simulations were carried out on different CPCs, taking into account effective working conditions and the presence of radiative heat transfer as well as the absence of adiabatic walls. The CFD model was validated considering a previous work reported in literature. The results were employed to develop some correlations by interpolation of numerical data, to express the Nusselt number on the receiver. We used these correlations to calculate heat losses of the receiver and to show the influence of different parameters such as the shape of receiver itself, tilt angle and concentration ratio. The variation of terms of the correlation as a function of characteristic length and concentration was studied. These results might be employed for a preliminary estimation procedure of a CPC collector efficiency and to propose sizingcriteria of general validity for this class of devices.

Introduction

Solar collectors are interesting solutions for different energy uses depending on the operating temperature. The use of flat plate collectors is suitable to collect thermal energy for domestic applications, while compound parabolic solar collectors (CPCs) can be employed when higher temperatures are required. Steam power level temperatures can be achieved by devices such as parabolic trough collectors (PTC), Fresnel collectors or solar dishes, which feature a higher concentration ratios but require more accurate tracking systems. In comparison with these last concentrators, an advantage of the CPC collectors is the possibility of operating with a moderate concentration without using a tracking system [1, 2].

Solar collectors can also have evacuated receivers to reduce convective heat transfer from the absorber, but with higher initial cost and complexity [3].

The heat transfer inside CPCs by radiation and natural convection is a complex function of geometrical dimensions, operating conditions and material properties [4]. Many studies have investigated the heat transfer and fluid dynamic phenomena, analyzing the interaction between surface radiation and natural convection inside simple cavities as described by Diaz et al. [5] and Mustafizur Rahman et al. [6].

Singh and Eames in [4] compared previous studies about flow inside CPCs reported in literature, and they concluded that the results were unrealistic: the reason was due to the assumptions of working conditions which were not achievable in real situations. Other authors, like Reichl et al. [5], investigated the flow pattern and heat transfer inside a CPC making a comparison between experimental and numerical results, to quantify contributions by each heat transfer mechanism.

This work was then developed with the aim of combining the methodologies described by Reichl et al. in [7] and Singh et al. in [4] with the aim of developing correlations to quantify the heat transfer between the absorber and the external environment, as a function of functional parameters and operative conditions.

Although this approach was derived from 2D numerical simulations with some simplifications and defined boundary conditions, nevertheless we maintain that it can be useful to understand the thermal performance of CPCs. In fact, as far as we know, there are no studies defining in an accurate way the relation between heat exchange in CPCs and operational parameters.

Nomenclature					
A_a		Area of aperture of collector $[m^2]$	**Subscript**		
A_i		Area exposed to sunlight $[m^2]$			
A_r		Total area of receiver $[m^2]$	c		Circular receiver
B		Parameter of correlation	f		Flat receiver
C		Concentration			
g		Acceleration due to Earth's gravity $[m/s^2]$			
Gr_H		Grashof Number based on the characteristic height H			
I		Solar constant $[W/m^2]$			
H		Height of collector $[m]$			
k		Thermal conductivity $[W/m * K]$			
L		Characteristic length of the geometry $[m]$			
n		Exponent of correlation			
Nu_L		Nusselt number based on the characteristic length L			
Pr		Prandtl number			
q''		Specific thermal heat losses of receiver $[W/m^2]$			
Q		Total thermal heat losses of receiver $[W]$			
Ra_H		Rayleigh number calculated respect to H			
T_a		Temperature of external environment [K]			
T_r		Temperature of receiver [K]			
α		Absorption coefficient of the receiver			
β		Volumetric thermal expansion coefficient $[1/K]$			
ε		Ratio between specific thermal heat losses evaluated for two different types of collector			
η		Thermal efficiency			
η'		Slope of the thermal efficiency			
η_{opt}		Optical efficiency			
ϑ		Tilt angle [deg]			
λ		Ratio between A_i and A_r			
ν		Kinematic viscosity $[m^2/s]$			
ρ		Reflection coefficient of the reflector			
σ		Product of the terms independent of temperature of the receiver			
τ		Transmission coefficient of the glass cover			
ω		Ratio between total thermal heat losses evaluated for two different types of collectors			

3. Methodology

3.1 Numerical model and solution method

In previously published works [4,7] the need for 3D simulations for the complete description of the motion field was evidenced. However, as stated by Reichl et al., [7]2D pseudo-transient simulations were able to provide reasonably accurate results with a much lower computational effort.

In this paper different models of CPCs, with different tilt angles and operating conditions were simulated. Each 2D CAD model, represented a cross section of a collector, was defined by its volume of air in the cavity, mirrors and insulation.

A mesh, as illustrated in Figure 1, was generated taking into account refinements near critical zones, such as the absorber and enclosure boundaries to solve the boundary layer [y+<=1] as suggested by Reichl et al.,[7]. A mesh quality sensitivity analysis was performed by employing 2D meshes with the number of elements ranging between 15000 and 70000.

The thickness of thin reflectors walls and glass cover was considered by setting the proper value in the software settings. Thicknesses of 1 mm for the reflector and 4 mm for the glass cover were used.

All calculations were performed using the ANSYS 14 code with double precision option enabled. The model includes radiative and convective exchanges, and it was assumed that solar radiation was completely absorbed by receiver. Buoyancy forces and a k-ε model were used, and the interaction between walls was then evaluated using enhanced wall treatment. Radiative heat transfer inside the collector was based on the surface to surface (S2S) model. The collector was assumed to be made of glass for the cover, polystyrene for the insulation, aluminum for the reflector and copper for the receiver. The physical properties of solid materials were considered constant with temperature. The air in the cavity was modeled as incompressible ideal gas.

At the boundary, cover glass and the insulation were respectively treated as mixed radiation and convection conditions; temperature of receiver was imposed by the user. An appropriate value of emissivity for the internal surfaces and cover glass was set, as reported in Table 1. An external heat transfer coefficient of 5 W/m^2K was defined taking into account an ambient temperature of 300 K.

Calculations were performed using the coupled algorithm and the body-force weighted discretization for pressure, while a second order upwind approach was followed for other quantities. We chose a pseudo-transient formulation and hybrid initialization, and the convergence criteria were fixed up to 10e-7 for energy and up to 10e-4 for the other physical variables.

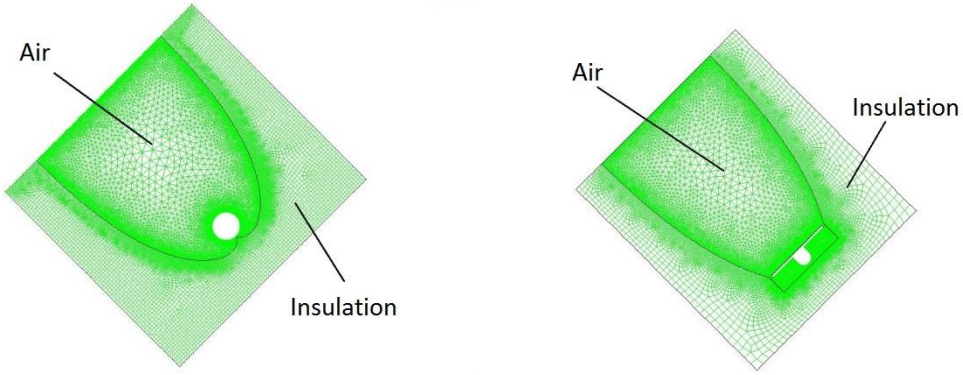

Figure 1: Mesh employed for CFD simulations of the investigated geometries.

Part	Emissivity	Material
Absorber	0.05	Copper with selective coating
Reflector	0.05	Aluminum
Cover	0.9	Glass

Table 1: Values of emissivity adopted for the numerical model.

3.2 Absorber shape and concentration

Two different shapes of receiver (flat and circular) were chosen and a concentration ratio of 2 was imposed; an unit axial depth was considered. The thickness of the surrounding polystyrene insulation was imposed to be directly proportional to the illuminated area cross section.
For the circular receiver the gap between receiver and bottom of enclosure was obtained joining two parabolas by a corner radius of 1 mm. Values of tilt angle, measured in relation to the ground, were chosen in the basis of the maximum annual collected energy: the range investigated was between 35 and 50 degrees. The receiver temperature ranged from T_a to 473 K. However, stagnation temperatures at the highest incident insolation (1000 W/m^2) were calculated for several concentration ratios . The lowest value was 500 K for a concentration ratio of 1.25, while the highest temperature, typical of a concentration ratio of 3, was 700 K.

3.3 General considerations

In this work the efficiency of the collectors was estimated as:

$$\eta = \eta_{opt} - \frac{Q}{IA_a} \quad (1)$$

For the optical efficiency a simplified approach was employed. Since the main focus of this paper is the thermal behavior, the optical efficiency was calculated by a balance of solar radiation inside the enclosure. Based on this approach, the optical efficiency was calculated as:

$$\eta_{opt_f} = \tau\alpha(\rho + \frac{1}{C}(1-\rho)) \qquad \eta_{opt_c} = \tau\alpha(\rho + \frac{1}{\pi C}(1-\rho)) \quad (1b)$$

Adopting a value of $\tau = 0.95$, $\alpha = 0.95$, $\rho = 0.95$, values of 0.88 and 0.86 were obtained for flat and circular geometry, respectively.
CFD simulations provided the values of total and radiative surface heat flux of the receiver. The heat exchange coefficient on the receiver was calculated as the ratio between the total thermal heat losses per square meter and the difference of temperature between receiver and the external environment. The heat transfer coefficient was used to obtain the Nusselt number employing an appropriate characteristic length.
The definition of the Grashof number was modified to take into account the geometry of the collector and tilt angle as follows:

$$Gr_H = \frac{\beta g H^3 \cos\vartheta (T_r - T_a)}{\nu^2} \qquad (2)$$

All fluid properties were estimated at film temperature to calculate the dimensionless quantities. Our aim was to determine two constants, B and n, in order to establish a correlation in the following form:

$$Nu_L = B(PrGr_H)^n = B(Ra_H)^n \quad (3)$$

Equation (3) described how convection and radiation affect heat transfer in a CPC, but it remained valid up to temperatures where the contribution of radiation was minimal. For higher temperatures it was necessary to separate the single effects.
The results showed that the values of B and n could be assumed practically constant up to a receiver temperature of 393 K. In fact, for higher values of this temperature limit, the slope of Nu_L was reduced. The reason was due to the increase of radiative heat transfer.
Equation (3) allowed for estimating efficiency variations as a function of receiver temperature. Thermal heat losses were expressed as:

$$Q = \frac{k}{L} B(Ra_H)^n A_r (T_r - T_a) \quad (4)$$

and, considering the expansion coefficient β as the reciprocal of film temperature, it was possible to write the efficiency as:

$$\eta = \eta_{opt} - \frac{BkA_r}{LA_a I}\left(\frac{2g\cos\vartheta PrH^3}{\nu^2}\right)^n \frac{(T_r - T_a)^{n+1}}{(T_r + T_a)^n} \qquad (5)$$

Differentiating Eq. 5 with respect to T_r and considering all properties constant with temperature , the result is the following:

$$\frac{d\eta}{dT_r} = \eta' = -\sigma\left(\frac{2nT_a}{T_r+T_a}+1\right)\left(\frac{T_r-T_a}{T_r+T_a}\right)^n \quad (6)$$

With

$$\sigma = \frac{BkA_r}{LA_aI}\left(\frac{2g\cos\vartheta H^3\mathrm{Pr}}{\nu^2}\right)^n \quad (7)$$

Equations (6) explains the reason why the slope of the efficiency curve is not linear with the temperature of receiver (see for instance Figure 5 in the following) as reported experimentally in literature. Considering that equation(3) was valid in a range of temperature between $T_a = 300$ K and $T_r = 393$ K, it was possible to note that for the upper values of this range the slope was less influenced by the temperature of receiver.

For very large temperatures η' reaches an asymptotic limit:

$$\lim_{T_r\to\infty} \eta' = -\sigma \quad (8)$$

i.e., the slope of efficiency reaches a negative constant.
We defined a parameter λ to distinguish the fraction of the illuminated area of the receiver with respect to the total area:

$$\lambda = \frac{A_i}{A_r} \quad (9)$$

For a circular receiver the illuminated area and the total area were the same ($\lambda_c = 1$), while for the flat one this ratio was lower than 0.5 as shown in Figure 2. Therefore, it was possible to express σ as:

$$\sigma = \frac{Bk}{ILC\lambda}\left(\frac{2g\cos\vartheta H^3\mathrm{Pr}}{\nu^2}\right)^n \quad (10)$$

highlighting that the variation of the efficiency could be related to construction parameters such as λ and C, as well as to the operating conditions represented by solar radiation and tilt angle.

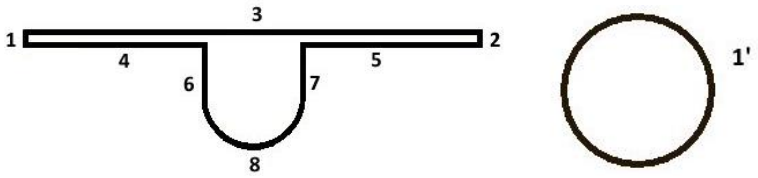

Figure 2: Scheme of flat receiver (left): the surface number 3 is the illuminated area A_i, while the union of all surfaces from 1 to 8 represents the total area of receiver A_r. For a circular receiver (right) the illuminated area and the total area are the same.

Analysis of results

In this section the main results are shown. Some comparisons to present more general results are made and main parameters, which influenced thermal heat exchange and flow pattern, are analyzed.

Comparison at same illuminated area

The performance of two collectors characterized by the same illuminated area and same concentrating ratio was studied. The flat receiver was compared with a circular geometry with different reference length. Both models were characterized by the same thickness of the insulation. Table 2 summarizes the main geometric features of investigated geometries.

receiver	flat	circular
characteristic size	width	diameter
L (m)	0.047	0.015
A_a (m^2)	0.1	0.1
H (m)	0.130	0.096
λ	0.42	1

Table 2: Geometric features of investigated geometries.

ϑ	B	N	
35	0.58	0.131	$5 \cdot 10^5 < Ra_H < 8.2 \cdot 10^6$
40	0.60	0.13	$4.7 \cdot 10^5 < Ra_H < 7.6 \cdot 10^6$
45	0.63	0.128	$4.3 \cdot 10^5 < Ra_H < 7 \cdot 10^6$
50	0.65	0.128	$3.9 \cdot 10^5 < Ra_H < 6.4 \cdot 10^6$

ϑ	B	n	
35	0.31	0.146	$2 \cdot 10^5 < Ra_H < 3.5 \cdot 10^6$
40	0.31	0.147	$1.9 \cdot 10^5 < Ra_H < 3.1 \cdot 10^6$
45	0.31	0.147	$1.8 \cdot 10^5 < Ra_H < 2.9 \cdot 10^6$
50	0.30	0.151	$1.6 \cdot 10^5 < Ra_H < 2.6 \cdot 10^6$

Table 3: Values of parameters B and n for flat geometry (left) and for circular geometry (right).

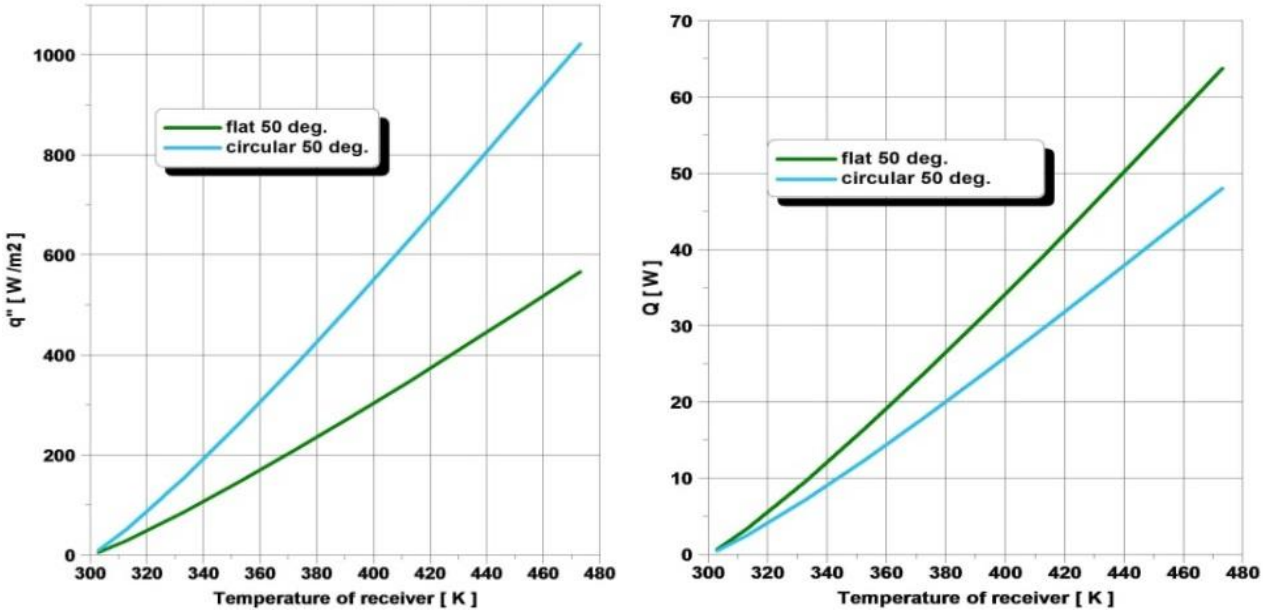

Figure 3: Specific (left) and total (right) thermal losses in function of temperature of receiver for the same value of illuminated area from 300 K until 473 K.

The ratio between specific thermal losses of circular and flat geometries was expressed as:

$$\varepsilon = \frac{q_c''}{q_f''} = \frac{h_c}{h_f} = \frac{B_c}{B_f}\frac{L_f}{L_c}\left(\frac{H_c}{H_f}\right)^{3n_f} Ra_{H_c}^{n_c - n_f} \qquad (11)$$

A quantity larger than unity was obtained for all tilt angles. On the other hand, the ratio ω between the total heat losses was lower than unity and it was influenced by the total surfaces of receivers expressed by the ratio between λ_f and λ_c. The effect of λ_f/λ_c proved to be prevailing on ε.

$$\omega = \frac{Q_c}{Q_f} = \varepsilon\frac{\lambda_f}{\lambda_c} \qquad (12)$$

In the analysed temperature range, both cases presented values of Ra_H of the same order of magnitude. In the investigated comparison specific thermal heat losses were greater for circular receiver, while the total heat losses were higher for the flat geometry, as illustrated in Figure 4.

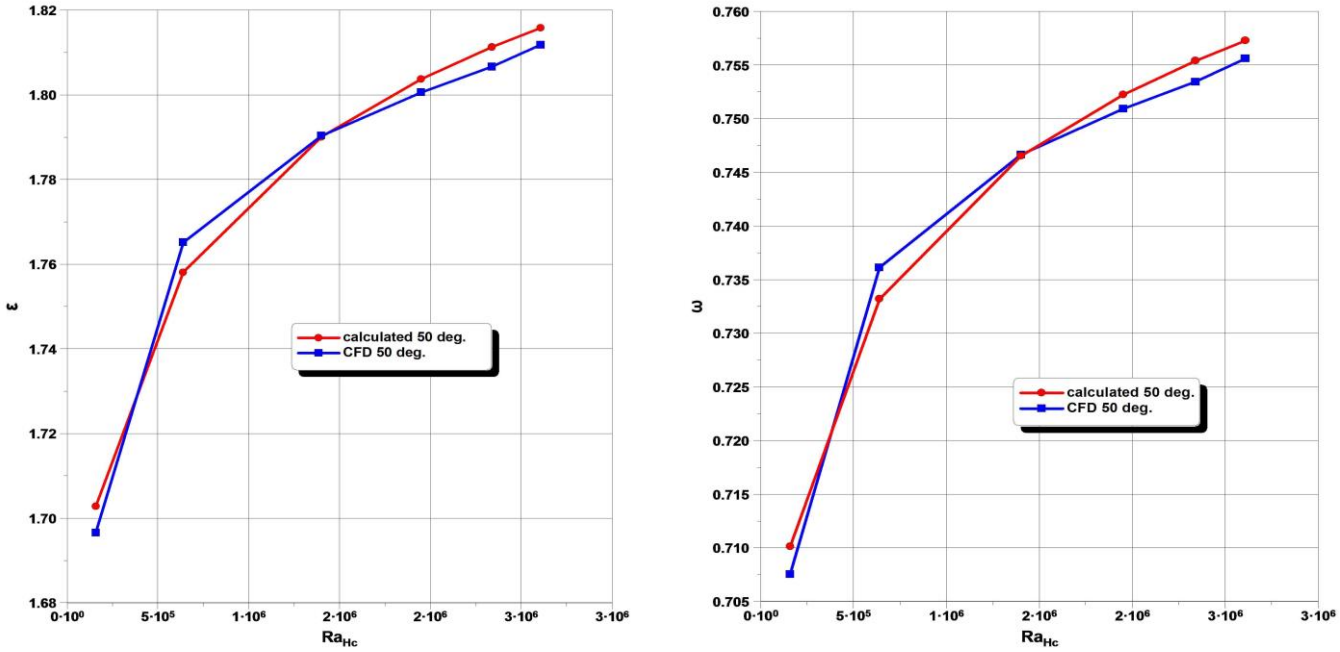

Figure 4: Trend of ε (left) and ω (right) obtained by correlation and CFD for a tilt of 50 degrees in the validity range of the correlations.

Due to the higher optical efficiency, the flat absorber performance was considered better than circular for temperatures below 340 K. Above this value, the circular shape was to be preferred.

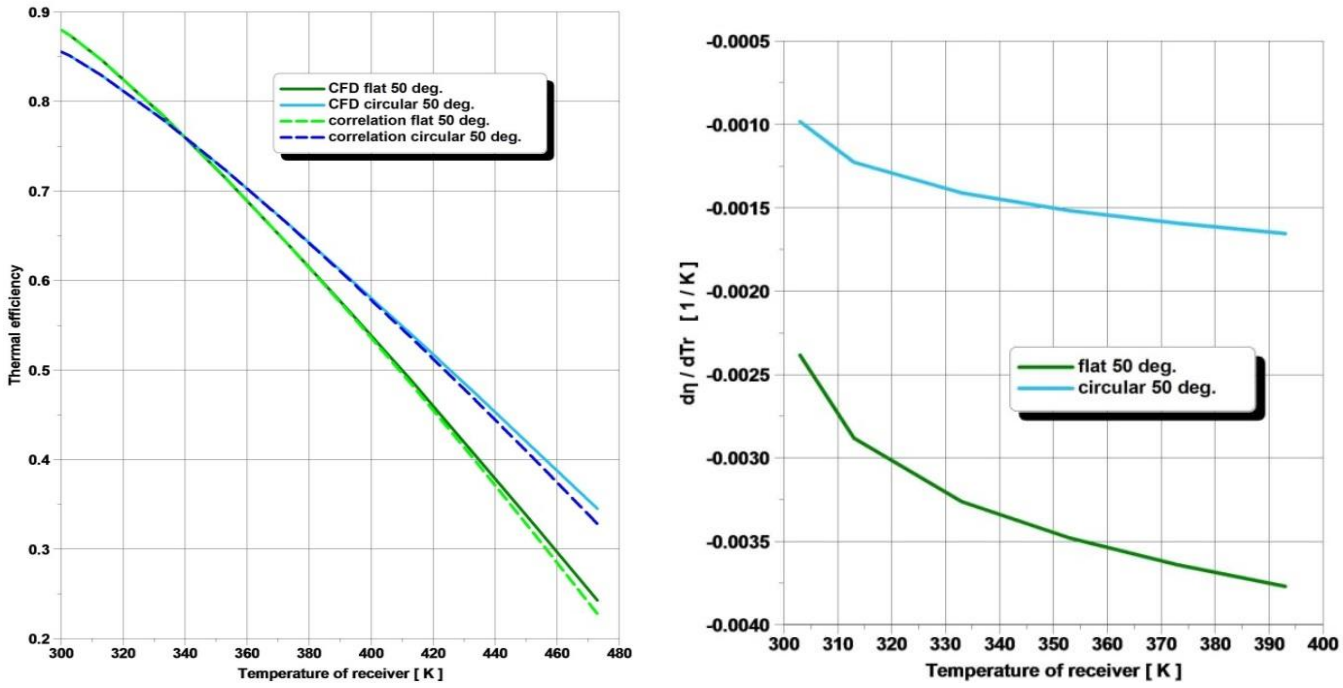

Figure 5: Thermal efficiency of flat and circular receiver obtained by CFD and by correlations (left) and its derivative (right).

Convection heat transfer depended on the values of tilt angle. In particular, an increase of the inclination made the fluid more unstable, entailing a larger spread of the thermal loop and showing different shapes of streamlines (Figures 6-9). This variation was more relevant for flat absorber and resulted in a variation of parameters B and n with tilt angle; in this case the specific thermal heat losses were more influenced by tilt. Near the receiver both cases presented a plume structure similar for both angles.

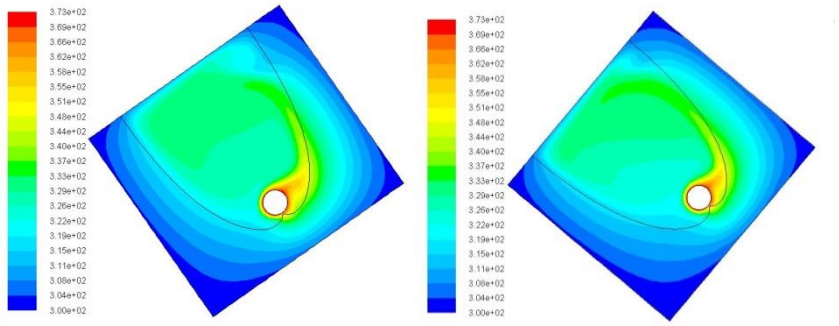

Figure 6: Isotherms at 373 K for ϑ=35 deg. (left) and ϑ=50 deg. (right) for circular receiver.

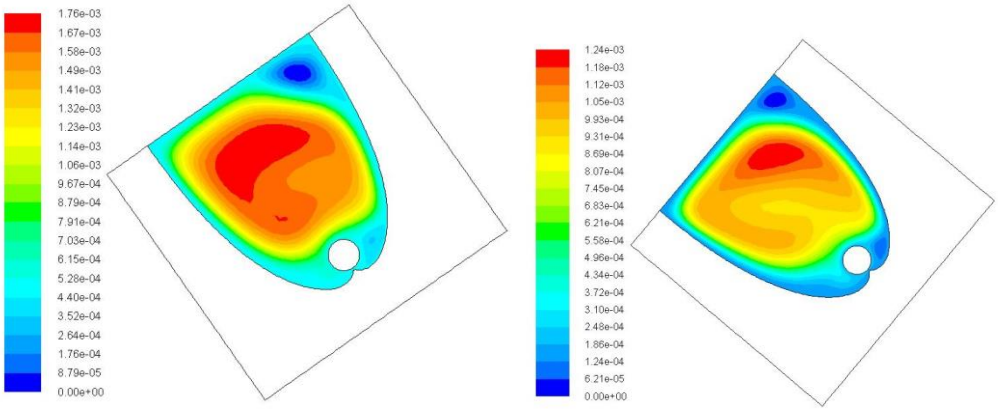

Figure 7: Streamlines at 373 K for ϑ=35 deg. (left) and ϑ=50 deg. (right) for circular receiver.

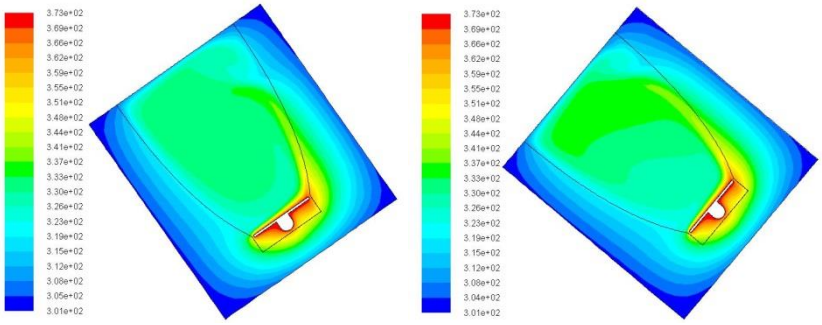

Figure 8: Isotherms at 373 K for ϑ=35 deg. (left) and ϑ=50 deg. (right) for flat receiver.

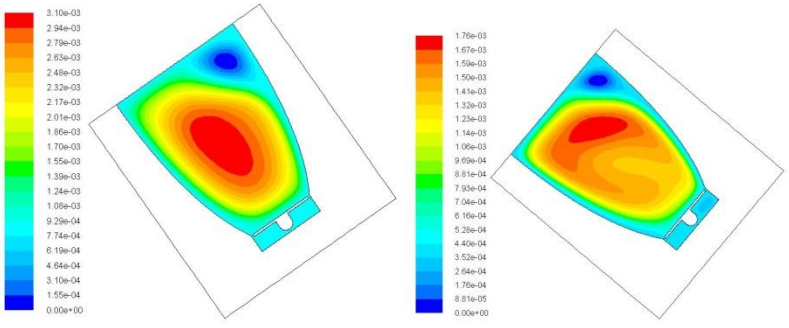

Figure 9: Streamlines at 373 K for ϑ=35 deg. (left) and ϑ=50 deg. (right) for flat receiver.

Circular absorber exchanged heat with surrounding air mainly by convection, while the flat receiver was characterized by a higher percentage of heat exchanged by radiation (Figure 10). This fact was due to both different shapes of the enclosures and different shapes of the absorbers, which entailed different values of view factors. The percentage of heat exchanged by convection reached a maximum value for a temperature of the receiver common to both geometries.

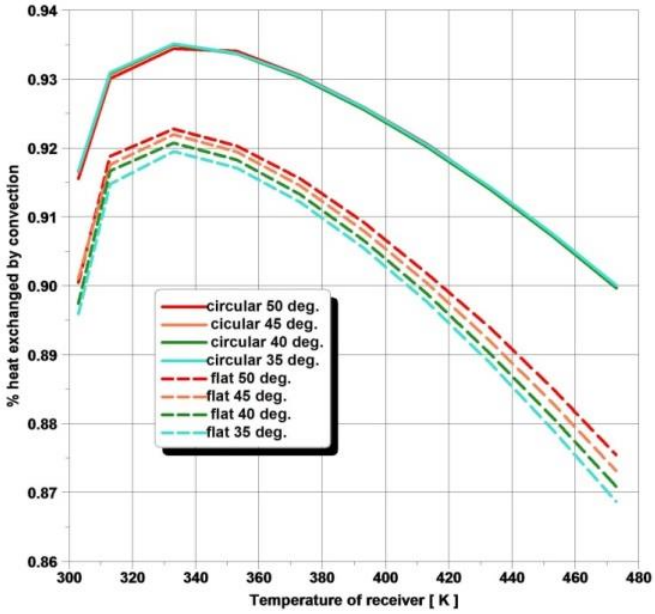

Figure 10: Percentage of heat exchanged by convection.

Analysis of the characteristic length at same concentration

The dependence of the parameters B and n of correlation (equation 3) was investigated by varying the values of characteristic length for a concentrating ratio of 2. Due to this reason, the diameter of the absorber was chosen in a range of values included between 15 and 70 mm. As an example, the results obtained with the circular geometry are presented in the following paragraph.

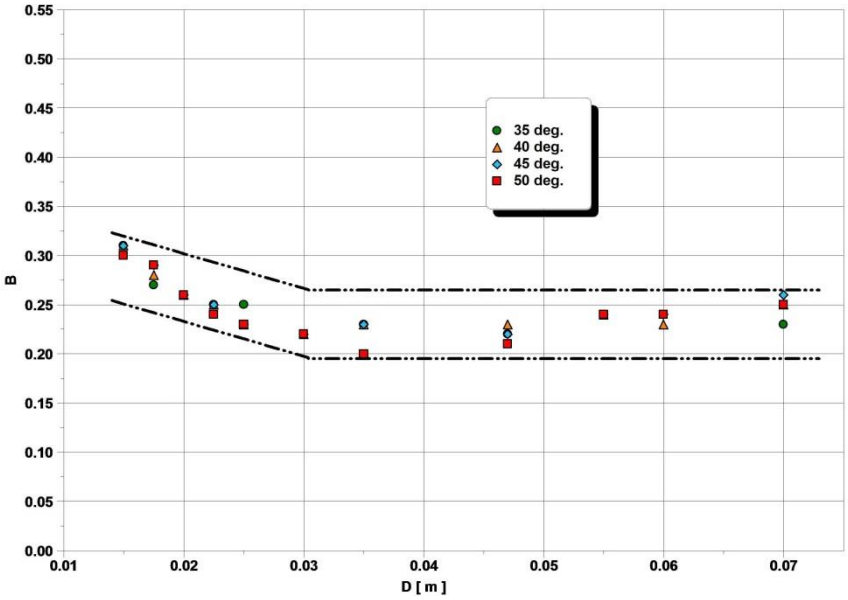

(a)

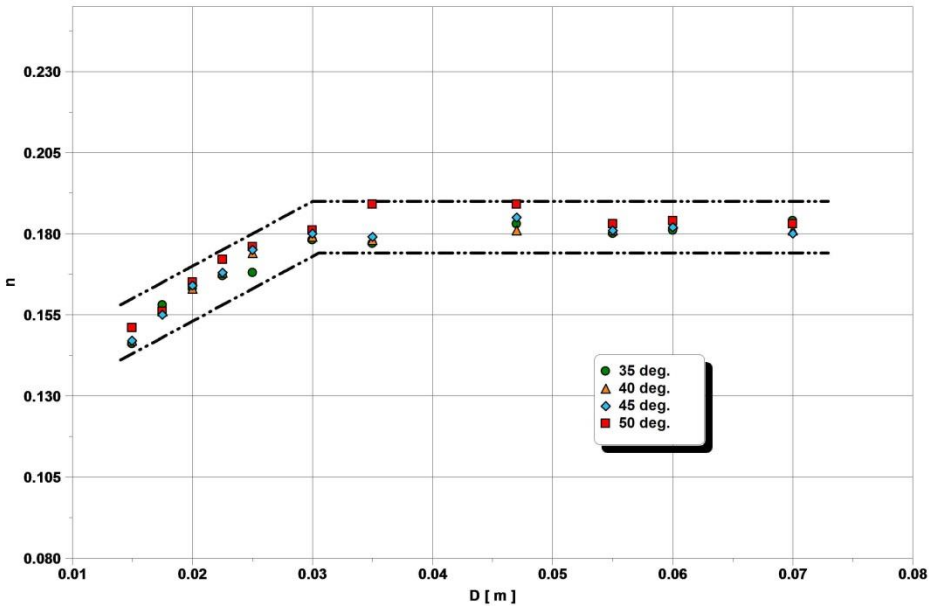

(b)

Figure 11: Trend of parameters B (a) and n (b) as a function of the diameter of the receiver.

As a result from Figure11, all values were confined in a band which was characterized by a change in slope. In fact, values of diameter lower than a critical one caused a negative slope for B and a positive slope for n, while, on the other hand, larger dimensions than the critical entailed a constant value for both quantities.
This behavior was due to differences in the motion of the filling air (Figures 12 and 13). In fact the gap between the bottom of the enclosure and the absorber was independent of absorber diameter. On the other hand, all other collector dimensions were directly proportional to the diameter of receiver. With smaller diameters, the filling air impinged the receiver and surrounded it passing through the gap; with larger diameters, instead, a larger amount of filling air surrounded the absorber but its motion was hindered by the gap. This is illustrated in figures 12-13-14.
It was therefore, clear that, near the absorber, small receiver diameters allowed the air to reach a value of velocity very close to the maximum, thus increasing the heat transfer. With larger diameters, instead, the velocity of the air was reduced so much to reduce the heat exchange considerably. A diameter close to 30 mm represented a borderline between these two different effects.

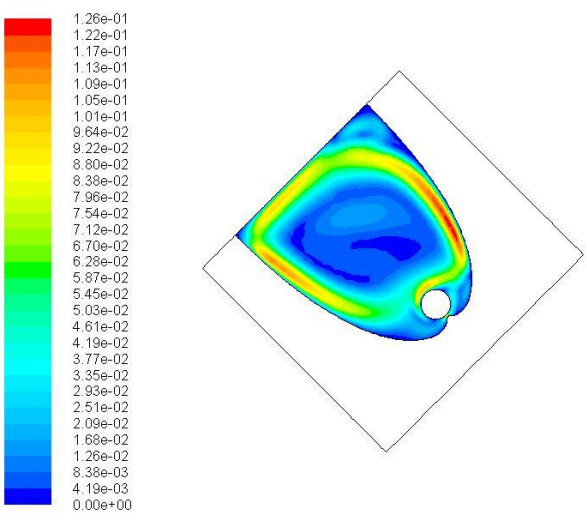

(a)

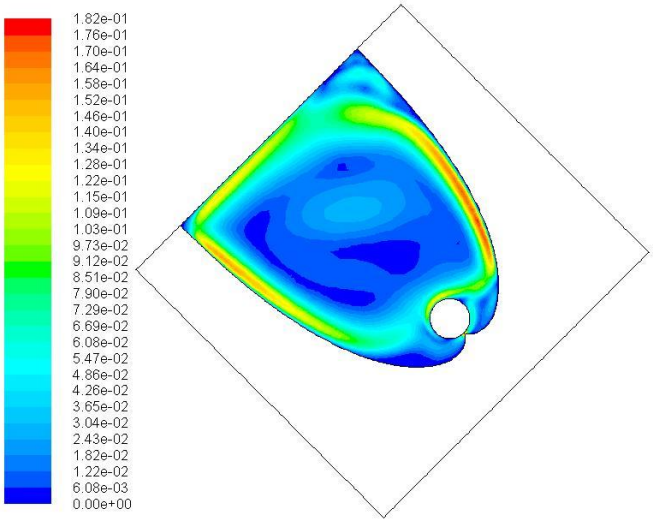

(b)

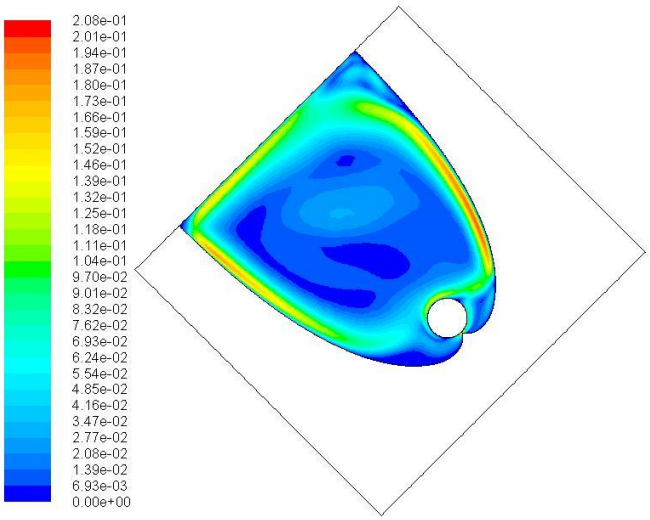

(c)

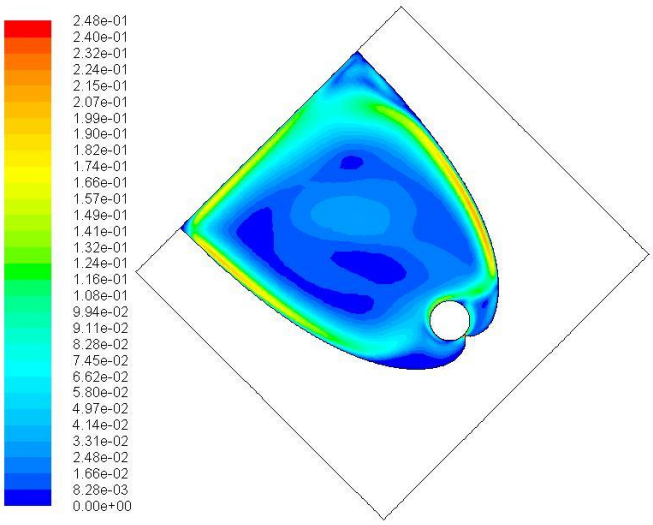

(d)

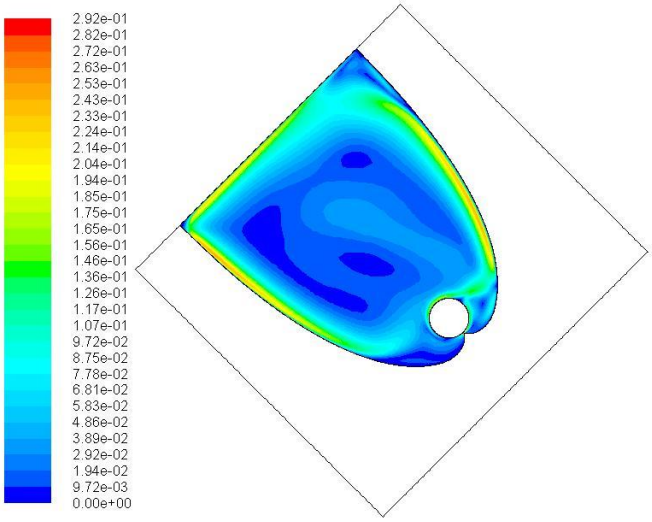

(e)

Figure 12: Contours of velocity magnitude [m/s] for diameter of 15 mm (a), 30mm (b) , 35mm (c), 47mm (d) and 70mm (e) for a temperature of 373 K and a tilt of 45 deg.

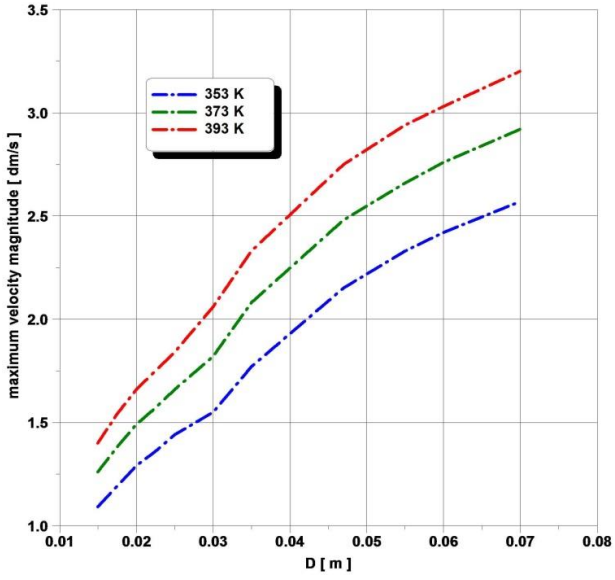

Figure 13: Maximum velocity magnitude as a function of the absorber diameter, for three receiver temperatures and constant tilt angle.

In the central part of the enclosure, the distribution of the contours of velocity magnitude was modified from smaller receiver diameters up to larger ones (Figure14); this was due to the restriction of the gap which promoted a stronger interaction between the air in contact with receiver and the remaining fluid in the central zone.

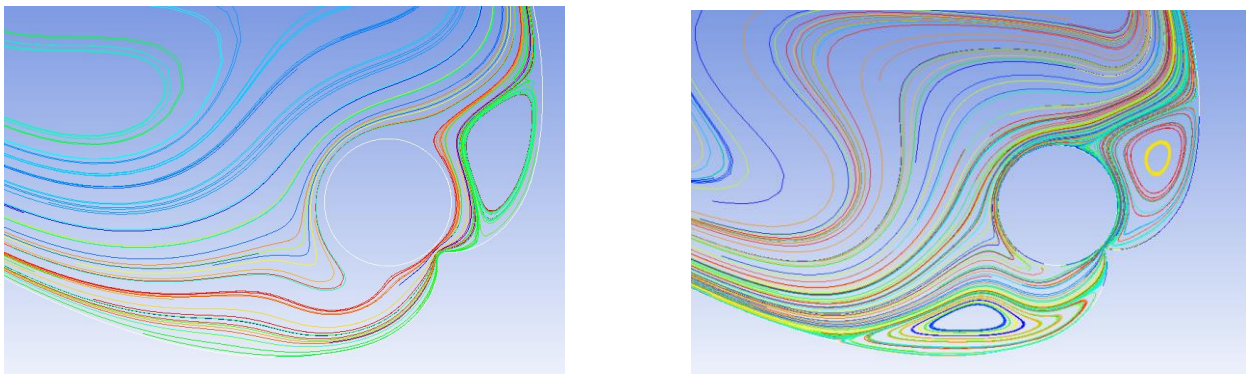

Figure 14: Pathlines for two different receiver diameters (15 mm on the left and 70 mm on the right) @ T_r = 373 K and Θ = 45 deg.

Effect of concentration ratio

CPCs with circular absorber were analysed to show effect of concentration on the terms of correlation (equation 3). We considered receivers characterized by different diameters, as summarized in Table 4, and a tilt angle of 35 degrees. Since the acceptance angle is depends on concentration ratio, in order to study devices able to collect the solar radiation with at least two seasonal adjustments, values of C up to 3 were considered [8].

Concentration	**Diameter [mm]**				
	15	**20**	**30**	**35**	**47**
1.25	31.4	42	62.9	73.4	98.6
1.5	50.6	67.7	101.5	118.5	159.1
1.7	67.6	90.4	135.6	158.2	212.5
2	96.4	128.8	193.2	225.5	302.8
2.5	153.3	205	307.4	358.7	481.7
3	221.8	296.6	444.9	519	697

Table 4: Values of heights in mm of the investigated collectors.

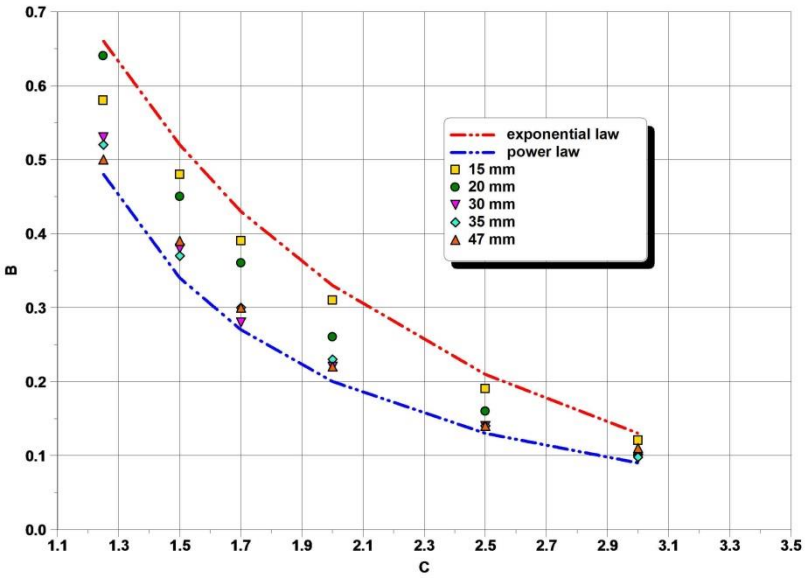

(a)

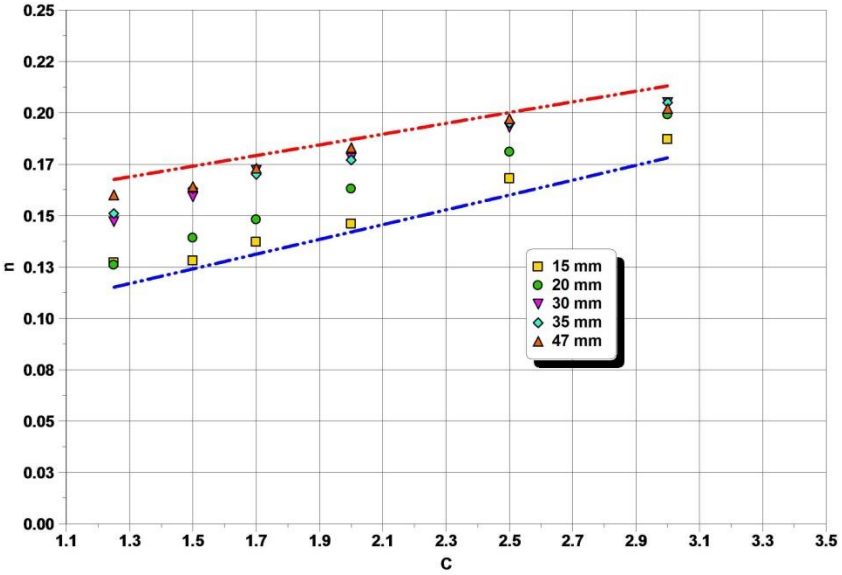

(b)

Figure 15: Trend of parameters B (a) and n (b) as a function of the concentrating ratio for different diameters.

The results of analyses shown that values of B (see Figure 15-a) were included in a band, which is a function of concentration ratio; in particular, the upper limit of the band was best-fitted by an exponential correlation, while the lower limit was characterized by a power law. Within the band, diameters lower than the critical value of 30 mm belonged to different exponential curves placed near the upper limit of the band. On the other hand, diameters larger than 30 mm were represented by overlapping points located in the lower part of the band and characterized by a power law trend.

The points representing the parameter n (Figure 15-b) were included in a band limited by two straight lines characterized by different slopes. Points associated with diameter lower than 30 mm followed two different lines, while those related to a diameter higher than this size overlapped. As discussed above, theseeffects were due to the dimensions of the gap between receiver and reflectors which prevented the motion of the filling air at high diameters.

It is worth noting that the structure of the internal flow for a concentration of 1.25 is different varying the diameter of the absorber. In fact sizes lower than 30 mm showed bicellular flow, while for other values the flow was unicellular. Other values of concentration were characterized by unicellular flow regardless of the sizes of the receiver. The reason is due to the ratio between diameter and height of enclosure as well as the imposed boundary conditions which influenced the flow structure, as reported in [4].

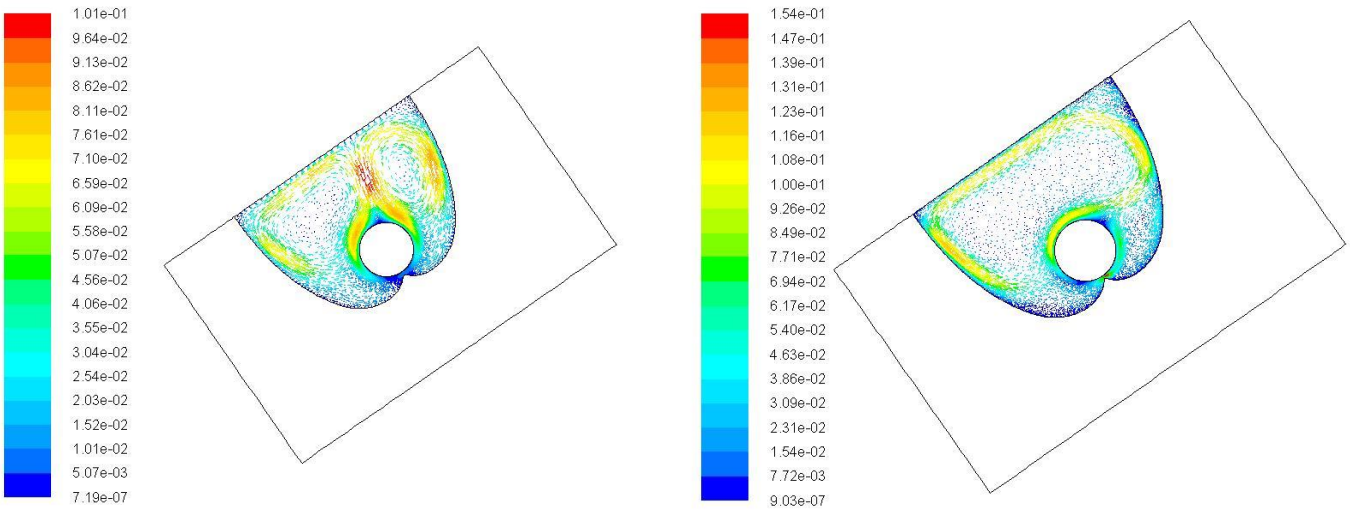

Figure 16: Vector velocity in [m/s] in a collectors with concentration of 1.25 for a diameter of 15mm (left) and 30 mm (right) at 373 K.

Conclusions

In this work the heat transfer in different CPCs, provided with flat or circular absorbers, was studied using results obtained by CFD simulations according to as suggested by Reichl et al. [7]. The aim of this study was to develop correlations in order to express the Nusselt number, calculated on the receiver, in function of the Rayleigh number, as a power law characterized by two parameters B and n. The resulting correlation is valid in the range from 300 K to 393 K and takes into account the convection and radiation heat transfer.
The obtained relationships can be easily used to express the influence of several terms, such as construction and operating parameters, on the efficiency.
Our findings suggested that the slope of the efficiency was less influenced by the temperature of the absorber when the temperature increases. In order to show the effect of construction parameters, two collectors were compared with the same concentration and the same value of receiving area, either with flat or circular absorbers. The results showed that the fraction of the illuminated surface influenced the value of total thermal losses; moreover, the heat transfer in case of circular shape was not dependent on tilt angle, and was characterized by a different percentage of radiative heat with respect to the flat one.
The variation of the coefficents contained in the correlation was also investigated as a function of the diameter of the receiver, keeping constant the concentration ratio. For each term a trend was obtained, which showed a discontinuity corresponding to a critical value of the diameter.
Some simulations were performed to express the coefficients of the correlation as a function of concentration ratio for different diameters. As a result, B was characterized by an exponential fitting curve for diameter smaller than the previously found critical value, while for larger values it was expressed by a power law. On the other hand, n was represented by straight lines with different slope.
These effects were due to the reduced gap between receiver and parabolas that, hindering the motion of air for diameters larger than the critical value, influenced the magnitude of heat transfer.
This work may provide useful correlations to design more efficient CPCs and to estimate its heat losses.

References

[1] M.Antonelli, A.Baccioli, M.Francesconi, R.Lensi, L.Martorano, Analysis of a low concentration solar plant with compound parabolic collectors and a rotary expander for electricity generation, (2014) Energy Procedia, 45, pp. 170-179.
[2] Antonelli, M., Baccioli, A., Francesconi, M., Desideri, U., Martorano, L. Electrical production of a small size Concentrated Solar Power plant with compound parabolic collectors (2015) Renewable Energy, 83, pp. 1110-1118.
[2] P. Horta, J.C.C. Henriques, M. Collares-Pereira, Impact of different internal convection control strategies in a non-evacuated CPC collector performance (2012) Solar Energy Vol. 86 pp. 1232-1244.
[3] H. Singh, P.C. Eames, A review of natural convective heat transfer correlations in rectangular cross-section cavities and their potential applications to compound parabolic concentrating (CPC) solar collector cavities, (2011) Applied Energy Vol.31 pp. 2186-2196.
[4] G. Diaz, R. Winston, Effect of surface radiation on natural convection in parabolic enclosures, (2008) Numerical Heat Transfer, Vol. 53, Part A, pp. 891-906.
[5]Md. Mustafizur Rahman1, M. A. Alim, Sumon Saha and M. K. Chowdhury, A numerical study of mixed convection in a square cavity with a heat conductong square cylinder at different locations, (2008) Journal of Mechanical Engineering Vol. ME.39, N°2.
[6] Ch. Reichl, F. Hengstberger, Ch. Zauner, Heat transfer mechanisms in a compound parabolic concentrator: comparison of computational fluid dynamics simulations to particle image velocimetry and local temperature measurements, (2013) Solar Energy Vol. 97 pp. 436-446.
[7] J.A. Duffie, W. A. Beckam, Solar Engineering of thermal processes, Wiley.
[8] A. Rabl, Comparison of solar concentrators, (1976), Solar Energy, Vol. 18, pp. 93-111.
[9] S.W. Churchill, H.H.S. Chu, Correlating equations for laminar and turbulent free convection from a horizontal cylinder, (1974) Heat Mass Transfer, Vol 18, pp 1049-1053.